Inorg. Chem. **2006**, *45*, 4431–4439

Homochiral Porous Lanthanide Phosphonates with 1D Triple-Strand Helical Chains: Synthesis, Photoluminescence, and Adsorption Properties

Qi Yue, Jin Yang, Guang-Hua Li, Guo-Dong Li, and Jie-Sheng Chen*

State Key Laboratory of Inorganic Synthesis and Preparative Chemistry, College of Chemistry, Jilin University, Changchun 130012, People's Republic of China

Received January 29, 2006

Four homochiral porous lanthanide phosphonates, $[Ln(H_2L)_3]\cdot 2H_2O$, (H_3L = (*S*)-HO_3PCH_2-NHC_4H_7-CO_2H, Ln = Tb (**1**), Dy (**2**), Eu (**3**), Gd (**4**)), have been synthesized under hydrothermal conditions. These compounds are isostructural, and they possess a 3D supramolecular framework built up from 1D triple-strand helical chains. Each of the helical chain consists of phosphonate groups bridging adjacent Ln(III) ions. The helical chains are stacked through hydrogen bonds to form 1D tubular channels along the *c* axis. Moreover, helical water chains are located in the 1D channels, and after removal of these water chains, the compounds exhibit selective adsorption capacities for N_2, H_2O, and CH_3OH molecules. Compounds **1** and **3** show strong green and red fluorescent emissions, respectively, in the solid state at room temperature. Crystal data for **1**: $TbP_3O_{17}N_3C_{18}H_{37}$, tetragonal (No.76), space group $P4_1$, a = 12.4643(3) Å, b = 12.4643(3) Å, c = 18.7577(5) Å, V = 2914.17(13) Å^3, and Z = 4. For **2**: $DyP_3O_{17}N_3C_{18}H_{37}$, a = 12.4486(3) Å, b = 12.4486(3) Å, c = 18.7626(5) Å, V = 2907.60(13) Å^3, and Z = 4. For **3**, $EuP_3O_{17}N_3C_{18}H_{37}$, a = 12.4799(3) Å, b = 12.4799(3) Å, c = 18.8239(5) Å, V = 2931.78(13) Å^3, and Z = 4. For **4**: $GdP_3O_{17}N_3C_{18}H_{37}$, a = 12.4877(18) Å, b = 12.4877(18) Å, c = 18.824(4) Å, V = 2935.5(8) Å^3, and Z = 4.

Introduction

The synthesis of inorganic−organic hybrid materials has attracted enormous attention because these extended systems play a significant role in catalysis, chirality, luminescence, magnetism, nonlinear optics, adsorption, and separation.[1,2] Recently, there has been interest in metal phosphonates, which are a special family of inorganic−organic hybrid compounds, because of their versatile structural features and potential applications.[3,4] A variety of metal phosphonates with an open-framework structure have been synthesized in the past decade, and these phosphonate compounds may exhibit microporosity for applications in adsorption and selective catalysis.[5,6] In addition, attaching functional groups to the phosphonic acid has led to the formation of metal phosphonates that possess functionalities within the micropores.[6,7−9] Nevertheless, the previously reported open-framework metal phosphonates mainly contain main-group metals or d-block transition metals as the framework component,[10−12] whereas open-framework (or microporous) lanthanide phosphonates are less common in the literature.[13−18] As lanthanide ions

* To whom correspondence should be addressed. E-mail: chemcj@jlu.edu.cn. Phone: +86-431-5168662. Fax: +86-431-5168624.

(1) Hagrman, P. J.; Hagrman, D.; Zubieta, J. *Angew. Chem., Int. Ed.* **1999**, *38*, 2639.
(2) Allcock, H. R. *Adv. Mater.* **1994**, *6*, 106.
(3) Clearfield, A. Metal Phosphonate Chemistry. In *Progress in Inorganic Chemistry*; Karlin, K. D., Ed.; John Wiley & Sons: New York, 1998; Vol. 47, pp 371−510 (and references therein).
(4) Clearfield, A. In *New Developments in Ion Exchange Materials*; Abe, M., Kataoka, T., Suzuki, T., Eds.; Kodansha, Ltd.: Tokyo, 1991.
(5) Odobel, F.; Bujoli, B.; Massiot, D. *Chem. Mater.* **2001**, *13*, 163.
(6) Evans, O. R.; Manke, D. R.; Lin, W.-B. *Chem. Mater.* **2002**, *14*, 3866.
(7) Zhang, B.; Clearfield, A. *J. Am. Chem. Soc.* **1997**, *119*, 2751.
(8) Clearfield, A.; Sharma, V. K.; Zhang, B. *Chem. Mater.* **2001**, *13*, 3099.
(9) Mao, J.-G.; Wang, Z.; Clearfield, A. *Inorg. Chem.* **2002**, *41*, 3713.
(10) Zhu, J.; Bu, X.; Feng, P.; Stucky, G. D. *J. Am. Chem. Soc.* **2000**, *122*, 11563.
(11) Kong, D.; Yang, L.; Xiang, O.; Prosvirin, A. V.; Zhao, H.; Ross, J. H., Jr.; Dunbar, K. M.; Clearfield, A. *Chem. Mater.* **2004**, *16*, 3020.
(12) Zheng, L.-M.; Gao, S.; Song, H.-H.; Decurtins, S.; Jacobson, A.-J.; Xin, X.-Q. *Chem. Mater.* **2002**, *14*, 3143.
(13) Ngo, H. L.; Lin, W.-B. *J. Am. Chem. Soc.* **2002**, *124*, 14298.
(14) Evans, O. R.; Ngo, H. L.; Lin, W.-B. *J. Am. Chem. Soc.* **2001**, *123*, 10395.
(15) Song, J.-L.; Lei, C.; Mao, J. G. *Inorg. Chem.* **2004**, *43*, 5630.
(16) Song, J.-L.; Mao, J. G. *Chem.—Eur. J.* **2005**, *11*, 1417.
(17) Serre, C.; Stock, N.; Bein, T.; Férey, G. *Inorg. Chem.* **2004**, *43*, 3159.

10.1021/ic060162h CCC: $33.50
Published on Web 04/28/2006

exhibit variable high coordination numbers, it is believed that the combination of lanthanide centers with phosphonate groups will result in unusual architectures, and unique properties resulting from f−f electronic transitions[19] may be found for the resulting materials.

Chiral inorganic−organic hybrid materials with microporous architectures are potentially applicable in enantioselective separation and asymmetric catalysis.[20−29] Therefore, it is of significance to incorporate enantiopure organic species that exhibit high homogeneous catalytic activity for asymmetric synthesis into the framework structures of microporous hybrid compounds. (*S*)-proline and its derivatives show high enantioselectivity in catalysis, and they are able to produce good yields in many catalytical reactions.[30−33] Although the past few years have witnessed significant advances in the synthesis of chiral d-block transition metal phosphonates with diverse structures using an enantiomerically pure derivative of (*S*)-proline, namely, *N*-(phosphonomethyl)proline, as the building unit,[34−36] the acquisition of functional chiral porous lanthanide phosphonates using *N*-(phosphonomethyl)proline as a chiral reactant has not been reported.

In this context, we chose the enantiomerically pure derivative of (*S*)-proline, *N*-(phosphonomethyl)proline, as a chiral building unit and successfully synthesized a series of homochiral porous lanthanide phosphonates consisting of one-dimensional triple-strand helical chains. These helical chains interact with one another through hydrogen bonds to form a 3D supramolecular framework with 1D tubular channels. Interestingly, the structural characterization reveals that there are one-dimensional helical water chains in the 1D channels. In addition, it is found that, after dehydration, the obtained compounds exhibit selective adsorption capacities for N_2 and other molecules. In this paper, the synthesis of $[Ln(H_2L)_3]\cdot 2H_2O$, (H_3L = (*S*)-HO_3PCH_2-NHC_4H_7-CO_2H; Ln = Tb (**1**), Dy (**2**), Eu (**3**), Gd (**4**)) and their adsorption and photoluminescence properties will be described.

Experimental Section

Materials. $EuCl_3\cdot 6H_2O$, $GdCl_3\cdot 6H_2O$, $TbCl_3\cdot 6H_2O$, and $DyCl_3\cdot 6H_2O$ were prepared by dissolving Eu_2O_3, Gd_2O_3, Tb_2O_3, and Dy_2O_3 in hydrochloric acid followed by drying and crystallization. Other reagents of analytical grade were obtained from a commercial source (No. 4 Chemical Factory, Tianjin, China) and used without further purification.

Synthesis of (*S*)-HO_3PCH_2-NHC_4H_7-CO_2H (H_3L). This compound was synthesized by following the procedure described in the literature.[37] Thus, 13 mmol (1.51 g) of L-proline, 26 mmol (2.13 g) of phosphorous acid, and 4 mL of hydrochloric acid (6.5 M in water) were loaded into a round-bottom flask fitted with a reflux condenser and heated for 5 min using a heating mantle. Formaldehyde (54 mmol, 1.5 mL, 36% aqueous solution) was added to this mixture. The solution was further refluxed for 90 min. Water was removed from the system by evacuation, and then 30 mL of ethanol was added. Continuous refluxing led to the formation of a white solid, which was subsequently recovered by filtration and dried in vacuo to yield the target compound (2.12 g, 78%).

Synthesis of $[Tb(H_2L)_3]\cdot 2H_2O$, 1. A mixture of $TbCl_3\cdot 6H_2O$ (0.112 g, 0.3 mmol) and H_3L (0.251 g, 1.2 mmol) was dissolved in 10 mL distilled water, followed by the addition of triethylamine until the pH value of the system was adjusted to about 2.0. The resulting solution was stirred for about 10 min at room temperature, sealed in a 23 mL Teflon-lined stainless steel autoclave, and heated at 100 °C for 2 days under autogenous pressure. Afterward, the reaction system was slowly cooled to room temperature. Colorless block crystals of **1** suitable for single-crystal X-ray diffraction analysis were collected from the final reaction system by filtration, washed several times with distilled water, and dried in air at ambient temperature. Yield: 46.7% based on Tb. Anal. Calcd for **1**: C, 26.36; H, 4.52; N, 5.13; Tb, 19.39. Found: C, 26.35; H, 4.51; N, 5.10; Tb, 19.35. Main IR bands (cm^{-1}): 3507m, 3382v, 3291v, 3240v, 3052m, 3003vs, 2854m, 2699v, 1701m, 1411m, 1358m, 1329m, 1148s, 1081s, 1043s, 1008s, 823m, 763s, 686v, 608v, 538s, 436s.

Synthesis of $[Dy(H_2L)_3]\cdot 2H_2O$, 2. Compound **2** was prepared in the same manner as compound **1**, using $DyCl_3\cdot 6H_2O$ (0.113 g, 0.3 mmol) instead of $TbCl_3\cdot 6H_2O$ as the metal source. Colorless block crystals were obtained in a 53% yield based on Dy. Anal. Calcd for **2**: C, 26.25; H, 4.50; N, 4.10; Dy, 19.75. Found: C, 26.24; H, 4.49; N, 4.08; Dy, 19.71. Main IR bands (cm^{-1}): 3506m, 3286v, 3050m, 2853m, 2658v, 1700m, 1410m, 1358m, 1329m, 1149m, 1082,s 1044s, 1009s, 824m, 763s, 688v, 608v, 544s, 436s.

Synthesis of $[Eu(H_2L)_3]\cdot 2H_2O$, 3. Compound **3** was prepared in a similar manner, and $EuCl_3\cdot 6H_2O$ (0.110 g, 0.3 mmol) was used as the metal source. Colorless block crystals were obtained in a 43% yield based on Eu. Anal. Calcd for **3**: C, 26.59; H, 4.55; N, 5.17; Eu, 18.71. Found: C, 26.56; H, 4.51; N, 5.15; Eu, 18.69. Main IR bands (cm^{-1}): 3508m, 3384v, 3052m, 2853m, 2698v, 1700m, 1410m, 1357m, 1328m, 1146s, 1080s, 1044s, 1007s, 824m, 763s, 687v, 609v, 539s, 436s.

Synthesis of $[Gd(H_2L)_3]\cdot 2H_2O$, 4. Compound **4** was successfully crystallized with $GdCl_3\cdot 6H_2O$ (0.111 g, 0.3 mmol) as the metal source using the procedure described above. Colorless block crystals were obtained in a 40% yield based on Gd. Anal. Calcd for **4**: C,

(18) Groves, J. A.; Wright, P. A.; Lightfoot, P. *Inorg. Chem.* **2005**, *44*, 1736.
(19) Antic-Fidancev, E.; Serpaggi, F.; Férey, G. *J. Alloys Compd.* **2002**, *340*, 88.
(20) Kepert, C. J.; Prior, T. J.; Rosseinsky, M. J. *J. Am. Chem. Soc.* **2000**, *122*, 5158.
(21) Kumagai, H.; Inoue, K. *Angew. Chem., Int. Ed.*. **1999**, *38*, 1601.
(22) Knof, U.; Zelewsky, A. *Angew. Chem., Int. Ed.* **1999**, *38*, 302.
(23) Porez-Garcua, L.; Amabilino, D. B. *Chem. Soc. Rev.* **2002**, *31*, 342.
(24) Seeber, G.; Pickering, A. L.; Long, D.-L.; Cronin, L. *Chem. Commun.* **2003**, 2002.
(25) Prior, T. J.; Rosseinsky, M. J. *Inorg. Chem.* **2003**, *42*, 1564.
(26) Inoue, K.; Imai, H.; Ghalsasi, P. S.; Kikuchi, K.; Ohba, M.; Kawa, H. O.; Yakhmi, J. V. *Angew. Chem., Int. Ed.* **2001**, *40*, 4242.
(27) Minguet, M.; Luneau, D.; Lhotel, E.; Villar, V.; Paulsen, C.; Amabilino, D. B.; Veciana, J. *Angew. Chem., Int. Ed*. **2002**, *41*, 586.
(28) Qin, C.; Xu, L.; Wei, Y.; Wang, X.; Li, F. *Inorg. Chem.* **2003**, *42*, 3107.
(29) Jouaiti, A.; Hosseini, M. W.; Kyritsakas, N. *Chem. Commun.* **2003**, 472.
(30) Bøgevig, A.; Juhl, K.; Kumaragurubaran, N.; Zhuang, W.; Jørgensen, K. A. *Angew. Chem., Int. Ed.* **2002**, *41*, 1790.
(31) Barrett, A. G. M.; Cook, A. S.; Kamimura, A. *Chem. Commun.* **1998**, 2533.
(32) Duthaler, R. O. *Angew. Chem., Int. Ed.* **2003**, *42*, 975.
(33) Dalko, P.; Moisan, L. *Angew. Chem., Int. Ed.* **2004**, *43*, 5138.
(34) Turner, A.; Jaffrws, P.-A.; MacLean, E. J.; Villemin, D.; Mckee, V.; Hix, G. B. *J. Chem. Soc., Dalton Trans.* **2003**, 1314.
(35) Yang, B.; Mao, J.; Sun, Y.; Zhao, H.; Clearfield, A. *Eur. J. Inorg. Chem.* **2003**, 4211.
(36) Shi, X.; Zhu, G.; Qiu, S.; Huang, K.; Yu, J.; Xu, R. *Angew. Chem., Int. Ed.* **2004**, *43*, 6482.
(37) Diel, P. J.; Maier, L. *Phosphorus, Sulfur Silicon Relat. Elem.* **1984**, *20*, 313.

Table 1. Crystal Data and Structure Refinements for Compounds **1**−**4**

	1	**2**	**3**	**4**
empirical formula	$TbP_3O_{17}N_3C_{18}H_{37}$	$DyP_3O_{17}N_3C_{18}H_{37}$	$EuP_3O_{17}N_3C_{18}H_{37}$	$GdP_3O_{17}N_3C_{18}H_{37}$
fw	819.34	822.92	812.38	817.67
wavelength (Å)	0.71073	0.71073	0.71073	0.71073
temp (K)	293(2)	293(2)	293(2)	293(2)
cryst syst	tetragonal	tetragonal	tetragonal	tetragonal
space group	$P4_1$ (No. 76)	$P4_1$ (No. 76)	$P4_1$ (No. 76)	$P4_1$ (No. 76)
a (Å)	12.4643(3)	12.4486(3)	12.4799(3)	12.4877(18)
b (Å)	12.4643(3)	12.4486(3)	12.4799(3)	12.4877(18)
c (Å)	18.7577(5)	18.7626(5)	18.8239(5)	18.824(4)
α (deg)	90	90	90	90
β (deg)	90	90	90	90
γ (deg)	90	90	90	90
V (Å^3)	2914.17(13)	2907.60(13)	2931.78(13)	2935.5(8)
Z	4	4	4	4
ρ_{calcd} (Mg/m^3)	1.867	1.880	1.840	1.850
μ (mm^{-1})	2.673	2.816	2.384	2.503
F(000)	1648	1652	1640	1644
reflns collected/unique	21 119/7231	21 153/7202	21 260/7013	28 885/6562
	R(int) = 0.0815	R(int) = 0.0597	R(int) = 0.0477	R(int) = 0.0610
cryst size (mm)	0.31 × 0.29 × 0.27	0.32 × 0.25 × 0.19	0.30 × 0.25 × 0.18	0.33 × 0.24 × 0.25
data/restraints/ params	7231/6/388	7202/5/391	7013/5/391	6562/6/391
GOF on F^2	0.971	1.001	1.044	1.093
Final R indices	R1 = 0.0403	R1 = 0.0302	R1 = 0.0245	R1 = 0.0326
[$I > 2\sigma(I)$]	wR2 = 0.0695	wR2 = 0.0558	wR2 = 0.0526	wR2 = 0.0586
R indices	R1 = 0.0521	R1 = 0.0372	R1 = 0.0294	R1 = 0.0396
(all data)	wR2 = 0.0731	wR2 = 0.0583	wR2 = 0.0550	wR2 = 0.0619
largest diff. peak	1.116 and	1.278 and	1.184 and	0.498 and
and hole (e A^{-3})	−0.564	−0.573	−0.554	−0.808

26.42; H, 4.53; N, 5.14; Gd, 19.24. Found: C, 26.39; H, 4.51; N, 5.12; Gd, 19.21. Main IR bands (cm^{-1}): 3508m, 3382v, 3052m, 2856m, 2700v, 1704m, 1410m, 1357m, 1329m, 1148s, 1081s, 1044s, 1007s, 823m, 762s, 685v, 608v, 538s, 434s.

Physical Measurements. The infrared spectra were recorded within the 400−4000 cm^{-1} region on a Bruker IFS 66V/S FTIR spectrometer using KBr pellets. The C, H, N elemental analyses were conducted on a Perkin-Elmer 240C element analyzer, whereas the thermogravimetric (TG) and differential thermal analysis (DTA) was performed on a Netzsch STA 449C thermogravimetric analyzer under an atmospheric environment at a heating rate of 20 °C/min. Inductively coupled plasma (ICP) analysis was conducted on a Perkin-Elmer Optima 3300DV ICP spectrometer. The powder X-ray diffraction (XRD) patterns were recorded on a Siemens D5005 diffractometer with Cu Kα radiation (λ = 1.5418 Å) over the 2θ range of 4−40° at room temperature; the recording speed was 0.3°/min. Nitrogen adsoption/desorption isotherms at the temperature of liquid nitrogen were obtained with a Micromeritics ASAP 2020M instrument after the samples were degassed at 200 °C and 1 × 10^{-5} Torr for 10 h prior to the measurements. The specific surface area was calculated using the BET equation, whereas the pore size distribution was determined from the desorption branch of the isotherm using the BJH method. The micropore surface area and micropore volume values were determined by the *t*-plot method from the volume adsorbed at a relative pressure of 0.4. The adsorption isotherms of H_2O and CH_3OH were obtained at 298 K by measuring the increase in weight at equilibrium as a function of relative pressure. These measurements were performed using a CAHN 2000 electrogravimetric balance. Prior to measurement, a known weight (typically 20−40 mg) of the as-synthesized sample was placed in a cylindrical Pt bucket and subjected to a programmed heating (250 °C, 2 h) in a vacuum to remove the guest water molecules. A point isotherm was recorded at the equilibrium state (the stage when no further weight change was observed). The photoluminescent properties of the samples were measured on a Perkin-Elmer LS55 spectrometer. To obtain good spectral resolution, a slit width of 2.5 nm was selected for both excitation and emission measurements.

Crystallographic Analyses. Crystallographic data of **1**−**4** were collected at room temperature on a Bruker-AXS Smart CCD diffractometer equipped with a normal-focus 2.4 kW X-ray source (graphite-monochromated Mo Kα radiation with λ = 0.71073 Å) operating at 50 kV and 40 mA with increasing ω (width of 0.3° and exposure time 30 s per frame). The structures were solved by direct methods using the program SHELXS-97[38] and refined by full-matrix least-squares against F^2 using the SHELXTL-97[39] crystallographic software package. All non-hydrogen atoms were easily found from the difference Fourier maps and refined anisotropically, whereas the hydrogen atoms of the organic molecules were placed by geometrical considerations and were added to the structure factor calculations. The H atoms on the water molecules of the compounds were located initially from the difference Fourier maps. However, the positions of these H atoms were adjusted by taking into account of the O−H bond distance values. Pertinent crystallographic data and structure refinement parameters for **1**−**4** are summarized in Table 1.

Results and Discussion

Selected bond distances and angles for compounds **1**, **2**, **3**, and **4** are listed in Tables 2−5. Compounds **2**, **3**, and **4** are isostructural with compound **1**, and therefore only the structure of **1** will be described in detail.

Crystal Structure. An ORTEP view of compound **1** is shown in Figure 1. Each asymmetric unit of **1** consists of one Tb(III) atom, three distinct H_2L^- anions, and two distinct lattice water molecules. The Tb(III) center is six-coordinated by phosphonate oxygen atoms from six H_2L^- anions in a

(38) G. M. Sheldrick, *SHELXS-97, Programs for X-ray Crystal Structure Solution*; University of Göttingen: Göttingen, Germany, 1997.
(39) G. M. Sheldrick, *SHELXTL-97, Programs for X-ray Crystal Structure Refinement*; University of Göttingen: Göttingen, Germany, 1997.

Table 2. Selected Bond Lengths (Å) and Angles (deg) for **1**[a]

Tb(1)−O(12)#1	2.239(4)	P(1)−C(5)	1.819(5)
Tb(1)−O(11)	2.268(4)	P(2)−O(6)	1.492(4)
Tb(1)−O(6)	2.274(4)	P(2)−O(7)	1.501(4)
Tb(1)−O(7)#1	2.274(4)	P(2)−O(8)	1.534(4)
Tb(1)−O(1)	2.274(4)	P(2)−C(11)	1.820(5)
Tb(1)−O(2)#2	2.289(4)	P(3)−O(11)	1.495(4)
P(1)−O(2)	1.493(4)	P(3)−O(12)	1.505(4)
P(1)−O(1)	1.508(4)	P(3)−O(13)	1.536(4)
P(1)−O(3)	1.555(4)	P(3)−C(17)	1.809(5)
O(12)#1−Tb(1)−O(11)	85.61(14)	O(3)−P(1)−C(5)	106.1(2)
O(12)#1−Tb(1)−O(6)	155.34(14)	O(6)−P(2)−O(7)	116.2(2)
O(11)−Tb(1)−O(6)	83.29(13)	O(6)−P(2)−O(8)	112.4(2)
O(12)#1−Tb(1)−O(7)#1	80.83(13)	O(7)−P(2)−C(11)	107.2(2)
O(11)−Tb(1)−O(7)#1	84.65(15)	O(6)−P(2)−C(11)	106.5(2)
O(6)−Tb(1)−O(7)#1	119.77(13)	O(7)−P(2)−C(11)	106.7(2)
O(12)#1−Tb(1)−O(1)	112.35(14)	O(8)−P(2)−C(11)	107.4(2)
O(11)−Tb(1)−O(1)	155.92(13)	O(11)−P(3)−O(12)	115.8(2)
O(6)−Tb(1)−O(1)	85.33(15)	O(11)−P(3)−O(13)	112.2(2)
O(7)#1−Tb(1)−O(1)	82.70(13)	O(12)−P(3)−O(13)	107.9(2)
O(12)#1−Tb(1)−O(2)#2	81.26(12)	O(11)−P(3)−C(17)	109.3(2)
O(11)−Tb(1)−O(2)#2	111.53(14)	O(12)−P(3)−C(17)	103.4(2)
O(6)−Tb(1)−O(2)#2	82.46(13)	O(13)−P(3)−C(17)	107.5(2)
O(7)#1−Tb(1)−O(2)#2	154.75(13)	P(1)−O(1)−Tb(1)	154.8(2)
O(1)−Tb(1)−O(2)#2	87.82(13)	P(1)−O(2)−Tb(1)#1	137.3(2)
O(2)−P(1)−O(1)	116.2(2)	P(2)−O(6)−Tb(1)	154.1(3)
O(2)−P(1)−O(3)	111.2(2)	P(2)−O(7)−Tb(1)#2	147.1(2)
O(1)−P(1)−O(3)	108.7(2)	P(3)−O(11)−Tb(1)	161.9(3)
O(2)−P(1)−C(5)	110.6(2)	P(3)−O(12)−Tb(1)#2	138.4(2)
O(1)−P(1)−C(5)	103.4(2)		

[a] Symmetry transformations used to generate equivalent atoms: #1 $-y+1, x-1, z+1/4$; #2 $y+1, -x+1, z-1/4$.

Table 3. Selected Bond Lengths (Å) and Angles (deg) for **2**[a]

Dy(1)−O(6)	2.234(3)	P(1)−C(5)	1.819(4)
Dy(1)−O(2)#1	2.252(3)	P(2)−O(6)	1.494(3)
Dy(1)−O(7)#1	2.255(3)	P(2)−O(7)	1.496(3)
Dy(1)−O(1)	2.261(3)	P(2)−O(8)	1.534(3)
Dy(1)−O(12)#2	2.270(3)	P(2)−C(11)	1.809(4)
Dy(1)−O(11)	2.274(3)	P(3)−O(11)	1.495(3)
P(1)−O(2)	1.502(3)	P(3)−O(12)	1.502(3)
P(1)−O(1)	1.504(3)	P(3)−O(13)	1.550(3)
P(1)−O(3)	1.534(3)	P(3)−C(17)	1.825(4)
O(6)−Dy(1)−O(2)#1	155.67(12)	O(3)−P(1)−C(5)	106.85(19)
O(6)−Dy(1)−O(7)#1	85.80(11)	O(6)−P(2)−O(7)	115.89(19)
O(2)#1−Dy(1)−O(7)#1	83.54(11)	O(6)−P(2)−O(8)	107.81(18)
O(6)−Dy(1)−O(1)	80.80(11)	O(7)−P(2)−O(8)	112.5(2)
O(2)#1−Dy(1)−O(1)	119.83(11)	O(6)−P(2)−C(11)	103.39(18)
O(7)#1−Dy(1)−O(1)	85.14(12)	O(7)−P(2)−C(11)	109.12(19)
O(6)−Dy(1)−O(12)#2	111.48(11)	O(8)−P(2)−C(11)	107.5(2)
O(2)#1−Dy(1)−O(12)#2	85.60(12)	O(11)−P(3)−O(12)	116.10(18)
O(7)#1−Dy(1)−O(12)#2	156.66(11)	O(11)−P(3)−O(13)	111.00(17)
O(1)−Dy(1)−O(12)#2	82.46(11)	O(12)−P(3)−O(13)	108.36(17)
O(6)−Dy(1)−O(11)	81.13(10)	O(11)−P(3)−C(17)	110.58(18)
O(2)#1−Dy(1)−O(11)	82.39(11)	O(12)−P(3)−C(17)	103.63(18)
O(7)#1−Dy(1)−O(11)	110.98(12)	O(13)−P(3)−C(17)	106.54(18)
O(1)−Dy(1)−O(11)	154.72(11)	P(1)−O(1)−Dy(1)	147.3(2)
O(12)#2−Dy(1)−O(11)	87.88(10)	P(1)−O(2)−Dy(1)#2	154.4(2)
O(2)−P(1)−O(1)	115.86(18)	P(2)−O(6)−Dy(1)	139.17(19)
O(2)−P(1)−O(3)	112.47(18)	P(2)−O(7)−Dy(1)#2	161.3(2)
O(1)−P(1)−O(3)	107.06(18)	P(3)−O(11)−Dy(1)	137.81(17)
O(2)−P(1)−C(5)	106.74(19)	P(3)−O(12)−Dy(1)#1	154.34(19)
O(1)−P(1)−C(5)	107.41(18)		

[a] Symmetry transformations used to generate equivalent atoms: #1 $y, -x+1, z-1/4$; #2 $-y+1, x, z+1/4$.

Table 4. Selected Bond Lengths (Å) and Angles (deg) for **3**[a]

Eu(1)−O(2)#1	2.279(3)	P(1)−C(5)	1.821(4)
Eu(1)−O(1)	2.292(3)	P(2)−O(6)	1.496(3)
Eu(1)−O(6)	2.294(3)	P(2)−O(7)	1.505(3)
Eu(1)−O(7)#1	2.297(2)	P(2)−O(8)	1.538(3)
Eu(1)−O(11)	2.309(3)	P(2)−C(11)	1.821(4)
Eu(1)−O(12)#2	2.313(2)	P(3)−O(12)	1.498(3)
P(1)−O(2)	1.491(3)	P(3)−O(11)	1.502(3)
P(1)−O(1)	1.499(3)	P(3)−O(13)	1.550(3)
P(1)−O(3)	1.544(3)	P(3)−C(17)	1.827(4)
O(2)#1−Eu(1)−O(1)	85.60(9)	O(3)−P(1)−C(5)	107.62(17)
O(2)#1−Eu(1)−O(6)	154.90(10)	O(6)−P(2)−O(7)	115.75(16)
O(1)−Eu(1)−O(6)	82.86(10)	O(6)−P(2)−O(8)	112.42(16)
O(2)#1−Eu(1)−O(7)#1	81.09(9)	O(7)−P(2)−O(8)	107.24(15)
O(1)−Eu(1)−O(7)#1	85.10(11)	O(6)−P(2)−C(11)	107.08(16)
O(6)−Eu(1)−O(7)#1	119.83(10)	O(7)−P(2)−C(11)	106.68(16)
O(2)#1−Eu(1)−O(11)	112.60(10)	O(8)−P(2)−C(11)	107.22(16)
O(1)−Eu(1)−O(11)	155.92(10)	O(12)−P(3)−O(11)	115.83(16)
O(6)−Eu(1)−O(11)	85.52(10)	O(12)−P(3)−O(13)	111.13(15)
O(7)#1−Eu(1)−O(11)	82.51(9)	O(11)−P(3)−O(13)	108.89(15)
O(2)#1−Eu(1)−O(12)#2	81.13(9)	O(12)−P(3)−C(17)	110.33(16)
O(1)−Eu(1)−O(12)#2	111.73(10)	O(11)−P(3)−C(17)	103.72(16)
O(6)−Eu(1)−O(12)#2	82.57(9)	O(13)−P(3)−C(17)	106.30(16)
O(7)#1−Eu(1)−O(12)#2	154.37(10)	P(1)−O(1)−Eu(1)	163.35(18)
O(11)−Eu(1)−O(12)#2	87.46(9)	P(1)−O(2)−Eu(1)#2	136.88(17)
O(2)−P(1)−O(1)	115.91(17)	P(2)−O(6)−Eu(1)	153.98(18)
O(2)−P(1)−O(3)	107.87(16)	P(2)−O(7)−Eu(1)#2	147.07(18)
O(1)−P(1)−O(3)	112.13(18)	P(3)−O(11)−Eu(1)	155.06(16)
O(2)−P(1)−C(5)	103.30(16)	P(3)−O(12)−Eu(1)#1	136.23(15)
O(1)−P(1)−C(5)	109.38(17)		

[a] Symmetry transformations used to generate equivalent atoms: #1 $-y+2, x, z+1/4$; #2 $y, -x+2, z-1/4$.

Table 5. Selected Bond Lengths (Å) and Angles (deg) for **4**[a]

Gd−O(6)	2.249(3)	P(1)−C(5)	1.827(5)
Gd−O(7)#1	2.282(4)	P(2)−O(7)	1.498(4)
Gd−O(12)#1	2.283(3)	P(2)−O(6)	1.505(4)
Gd−O(11)	2.287(3)	P(2)−O(8)	1.545(4)
Gd−O(1)	2.293(3)	P(2)−C(11)	1.818(5)
Gd−O(2)#2	2.293(3)	P(3)−O(12)	1.504(4)
P(1)−O(2)	1.508(4)	P(3)−O(11)	1.509(4)
P(1)−O(1)	1.509(3)	P(3)−O(13)	1.538(3)
P(1)−O(3)	1.553(3)	P(3)−C(17)	1.826(5)
O(6)−Gd−O(7)#1	85.81(13)	O(3)−P(1)−C(5)	106.2(2)
O(6)−Gd−O(12)#1	155.52(13)	O(7)−P(2)−O(6)	115.3(2)
O(7)#1−Gd−O(12)#1	83.16(13)	O(7)−P(2)−O(8)	111.4(2)
O(6)−Gd−O(11)	80.96(13)	O(6)−P(2)−O(8)	109.1(2)
O(7)#1−Gd−O(11)	84.99(15)	O(7)−P(2)−C(11)	109.5(2)
O(12)#1−Gd−O(11)	119.56(12)	O(6)−P(2)−C(11)	103.3(2)
O(6)−Gd−O(1)	81.03(11)	O(8)−P(2)−C(11)	107.7(2)
O(7)#1−Gd−O(1)	111.62(14)	O(12)−P(3)−O(11)	116.1(2)
O(12)#1−Gd−O(1)	82.85(12)	O(12)−P(3)−O(13)	111.4(2)
O(11)−Gd−O(1)	154.40(13)	O(11)−P(3)−O(13)	107.9(2)
O(6)−Gd−O(2)#2	112.22(13)	O(12)−P(3)−C(17)	107.0(2)
O(7)#1−Gd−O(2)#2	156.03(12)	O(11)−P(3)−C(17)	106.6(2)
O(12)#1−Gd−O(2)#2	85.26(14)	O(13)−P(3)−C(17)	107.5(2)
O(11)−Gd−O(2)#2	82.59(13)	P(1)−O(1)−Gd	136.6(2)
O(1)−Gd−O(2)#2	87.57(12)	P(1)−O(2)−Gd#1	154.8(2)
O(2)−P(1)−O(1)	116.1(2)	P(2)−O(6)−Gd	138.4(2)
O(2)−P(1)−O(3)	108.7(2)	P(2)−O(7)−Gd#2	162.7(2)
O(1)−P(1)−O(3)	111.1(2)	P(3)−O(11)−Gd	147.1(2)
O(2)−P(1)−C(5)	103.6(2)	P(3)−O(12)−Gd#2	153.8(2)
O(1)−P(1)−C(5)	110.5(2)		

[a] Symmetry transformations used to generate equivalent atoms: #1 $-y+1, x-1, z+1/4$; #2 $y+1, -x+1, z-1/4$.

severely distorted octahedral coordination sphere. The distances of the Tb−O bonds range from 2.239(4) to 2.289(4) Å. There are three sets of O−Tb−O bond angles in the ranges of 80.83(13)−87.82(13), 112.35(14)−119.77(13), and 154.75(13)−155.92(13)°. It is noteworthy that the three distinct H_2L^- anions in the asymmetric unit of **1** adopt the same coordination mode: only one phosphonate oxygen atom is protonated, and another two of the three phosphonate oxygen atoms coordinate to two adjacent Tb(III) centers in a monodentate manner. The carboxylate group of the H_2L^-

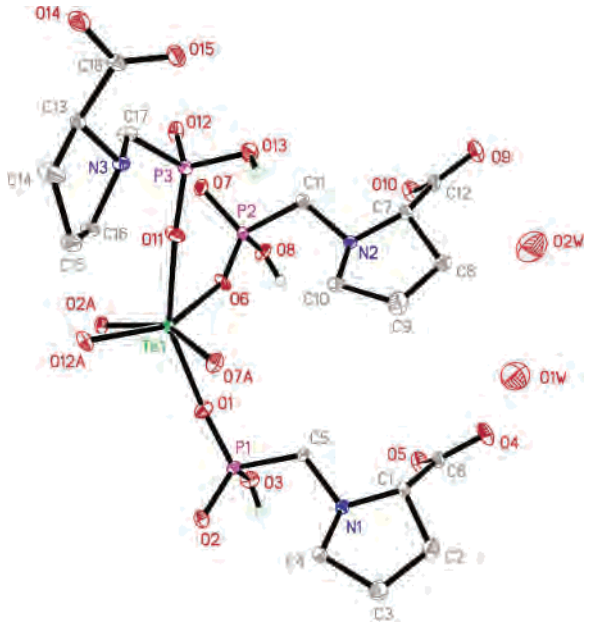

Figure 1. ORTEP view of compound **1** with 50% thermal ellipsoids. The small green open circles represent the hydrogen atoms attached to the phosphonate oxygen atoms, whereas the hydrogen atoms attached to nitrogen atoms, carbon atoms, and lattice water molecules are omitted for clarity.

anions is deprotonated, but it does not coordinate to the Tb(III) center. The geometry about each phosphorus atom is slightly distorted from tetrahedral with the O−P−O and O−P−C angles being from 107.2(2) to 116.2(2)° and 103.4(2) to 110.6(2)°, respectively. The P−$O_{bridging}$ bond lengths are in the range of 1.492(4)−1.508(4) Å, and the protonated P−OH bond lengths are in the range of 1.534(4)−1.555(4) Å, which are slightly longer than those of deprotonated P−O groups. A strong absorption band in the range of 938−1149 cm^{-1}, a weak one at 824 cm^{-1}, and a medium one at around 763 cm^{-1} in the infrared spectrum of **1** can be attributed to the stretching vibrations of P−O, P−OH, and P−C of the phosphonate group, respectively.[40]

In compound **1**, the Tb(III) centers are interconnected by bridging phosphonate groups of the H_2L^- anions to form infinite one-dimensional helical chains running along the *c* axis with a Tb···Tb separation of 4.8945 Å. Interestingly, each helical chain is constructed by right-handed triple-strands formed from three phosphonate groups of three H_2L^- species which bridge two adjacent Tb(III) ions along the crystallographic 4_1 screw axis (Figure 2a and 2c). An individual strand of the triple helix has a repeat unit consisting of Tb−O−P1−O−Tb−O−P2−O−Tb−O−P3−O−Tb−O−P1−O with a period of 18.758 Å. The organic moieties of the phosphonate groups appear to be leaves pointing outward from the triple-strand helical chain, and the pyrrolidinyl ring is approximately perpendicular to the helical chain. The adjacent triple-strand helical chains are further assembled through O−H···O and N−H···O hydrogen bonds into a 3D supramolecular framework featuring 1D tubular channels with a free diameter of about 4.32 × 3.81 Å (defined by the separation between the nearest diagonal H atoms, and van der Waals radius of the H atoms is taken into account) (Figure 2b and 2d). The protonated phosphonate oxygen atoms (O(3), O(8), and O(13)) of three H_2L^- anions act as the hydrogen donors and form O−H···O hydrogen bonds with the carboxylate oxygen atoms of the H_2L^- anions (O(9)#3, O(14)#4, and O(4)#5) as the hydrogen acceptors in neighboring helical chains (Table 6). Simultaneously, the hydrogen atoms attached to the N atoms of the H_2L^- anions (N(1), N(2), and N(3)) in the helical chain interact with the carboxylate oxygen atoms of the H_2L^- anions (O(10)#3, O(15)#4, and O(5)#5) in neighboring helical chains to form N−H···O hydrogen bonds, giving rise to a hydrogen-bonded right-handed helical chain running along the *c* axis (Figure 3a). The hydrogen-bonding distances of O−H···O (2.442(5), 2.449(5), and 2.543(6) Å) and N−H···O (2.700(6), 2.782(6), and 2.865(6) Å) are slightly shorter than those reported in the literature (mean O···O and N···O distances are 2.765 and 2.946 Å, respectively). These strong hydrogen-bonding interactions in compound **1** are favorable for stabilization of the 3D supramolecular framework.

A notable feature for the compound is the presence of helical water chains, and it is believed that the helical host acts as a template for the formation of the helical chains of water molecules. Among various types of water clusters, 1D chain arrangements of water molecules are of interest because of their occurrence in several biological processes related to water and ion transport.[41] Nevertheless, the knowledge of structural constraints required in the stabilization of water chains and the effect of chain structures on the host remains incomplete. In **1**, the one-dimensional helical water chain with a pitch of 18.758 Å runs along the crystallographic 4_1 screw axis, and two types of lattice water molecule in the water chain are arranged in an ABAB fashion (Figure 3a). The water chains are stabilized by hydrogen bonds. The interatomic distances and angles for the hydrogen-bonding interactions in **1** are presented in Table 6. The O(2w) molecule only acts as a donor, while the O(1w) molecule only as an acceptor in the helical water chain, with the O(2w)···O(1w) and O(2w)···O(1wA) distances being 2.903(9) and 2.782(9) Å, respectively. The angles O(2w)−O(1w)−O(2wA) and O(1w)−O(2w)−O(1wA) in the water helix are 115.611 and 117.253°, respectively. Meanwhile, the helical water chains are anchored onto the triple-strand helical host chains, through hydrogen-bonding interactions (O1w···O4 = 2.963(7) Å) between the noncoordinating carboxylate oxygen atom (O4) and one of the water molecules (O1w) (Figure S1 in the Supporting Information). Interestingly, such weak interactions with the right-handed helical host chains induce a left-handed helicity of water chains (Figure 3b and c). In a sense, the formation of the helical water chains depends on the chemical information and structure of the helical host chains. Furthermore, the hydrogen-bonding acceptors (carboxylate oxygen atoms) in **1** are in a favorable position for anchoring different water molecules into an extended array. In fact, the hydrogen bonds play an important role not only in the formation of the water chains but also in the stabilization of the supramolecular framework after removal of the water chains. As demonstrated later, the

(40) Fu, R.; Xiang, S.; Zhang, H.; Zhang, J.; Wu, X. *Cryst. Growth Des.* **2005**, *5*, 1795.

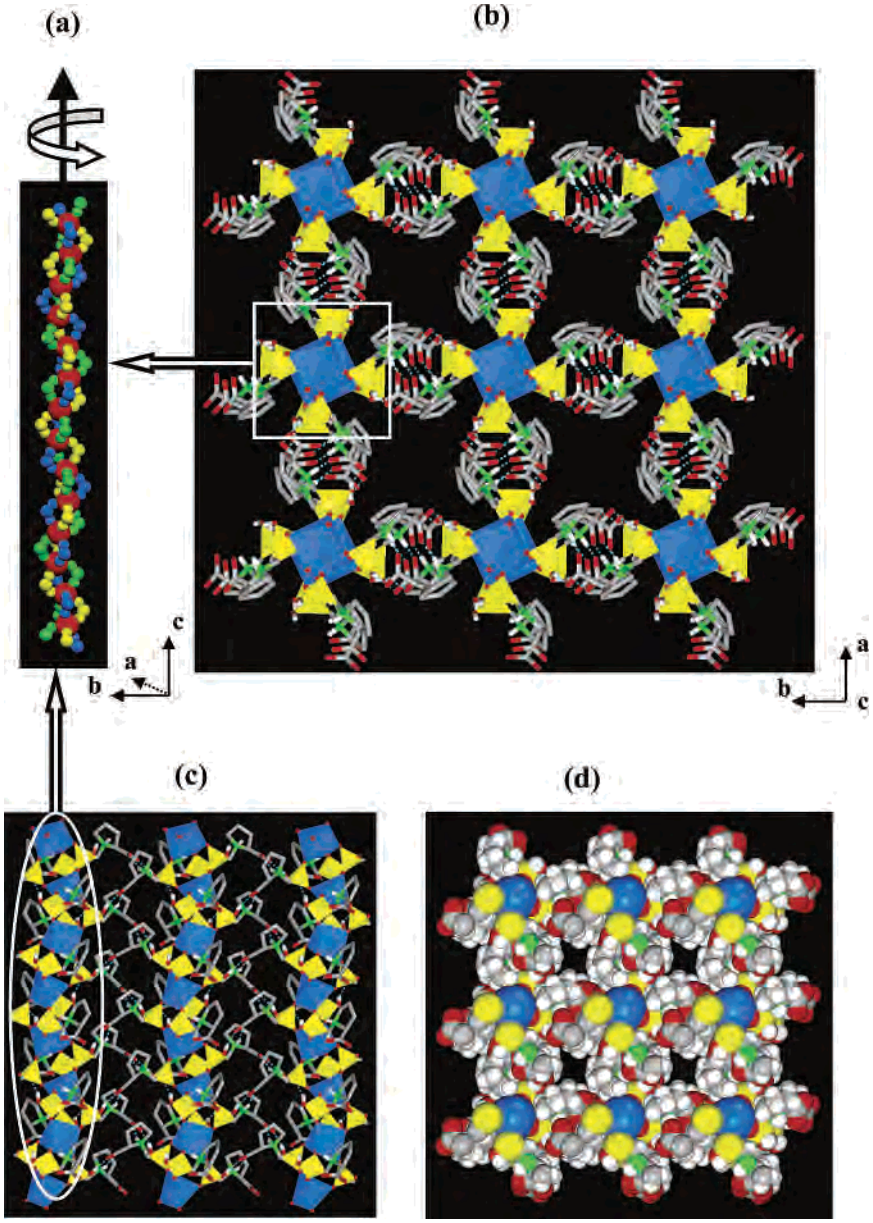

Figure 2. Helical chain structure in **1** running along the crystallographic 4_1 axis (the organic moieties of H_3L are omitted for clarity) (a), the 3D supramolecular framework of **1** viewed along the *c* (b) *a* axes (c), and the space filling structure of **1** viewed along the *c* axis (d). The arrows in panel a indicate the helicity of the chain; the hydrogen atoms attached to carbon atoms are omitted for clarity, and the hydrogen bonds are indicated by the dotted lines: Tb, blue; P, yellow; C, gray; N, green; O, red; H, white.

Table 6. Interatomic Distances and Angles for the Hydrogen Bonds in **1** (Å and deg)[a]

D−H···A	*d*(D−H)	*d*(H···A)	*d*(D···A)	∠(DHA)
O(3)−H(3)···O(9)#3	0.82	1.77	2.543(6)	156.0
O(8)−H(8)···O(14)#4	0.82	1.74	2.449(5)	144.2
O(13)−H(13)···O(4)#5	0.82	1.74	2.442(5)	141.9
O(13)−H(13)···O(5)#5	0.82	2.57	3.353(6)	159.0
O(1W)−H(1WA)···O(4)	0.89(2)	2.08(3)	2.963(7)	171(7)
O(2W)−H(2WA)···O(1W)	0.91(2)	2.11(6)	2.903(9)	145(8)
O(2W)−H(2WB)···O(1W)#5	0.866(6)	1.916(6)	2.782(9)	178.0(5)
N(1)−H(1)···O(10)#3	0.91	1.85	2.700(6)	153.6
N(2)−H(2)···O(15)#4	0.91	1.95	2.782(6)	152.0
N(3)−H(3A)···O(5)#5	0.91	2.03	2.865(6)	152.6

[a] Symmetry transformations used to generate equivalent atoms: #1 $-y+1, x-1, z+1/4$; #2 $y+1, -x+1, z-1/4$; #3 $-x+2, -y+1, z+1/2$; #4 $-y+1, x, z+1/4$; #5 $y, -x+1, z-1/4$.

compound shows porosity upon heating which leads to the removal of the water molecules occluded in the as-synthesized compound. Porosity sustained by H-bonds has been occasionally observed[42] for other metal−organic compounds, but examples containing helical phosphonate chains were not reported to the best of our knowledge. The infrared spectrum of **1** shows two weak broad bands centered at around 3506 and 3379 cm^{-1}, as well as a very weak broad band at around 3288 cm^{-1}, attributable to the O−H stretching vibrations of the water molecules. The O−H stretching vibration in liquid water appears at 3490 and 3280 cm^{-1}. Hence, the O−H stretching vibration of water molecules in the water chain of **1** are similar to those in liquid water,[43]

(41) Lou, B.; Jiang, F.; Yuan, D.; Wu, B.; Hong, M. *Eur. J. Inorg. Chem.* **2005**, 3214.
(42) (a) Sreenivasulu, B.; Vittal, J. J. *Angew. Chem., Int. Ed.* **2004**, *43*, 5769. (b) Mukherjee, A.; Saha, M. K.; Nethaji, M.; Chakravarty, A. R. *Chem. Commun.* **2004**, 716.

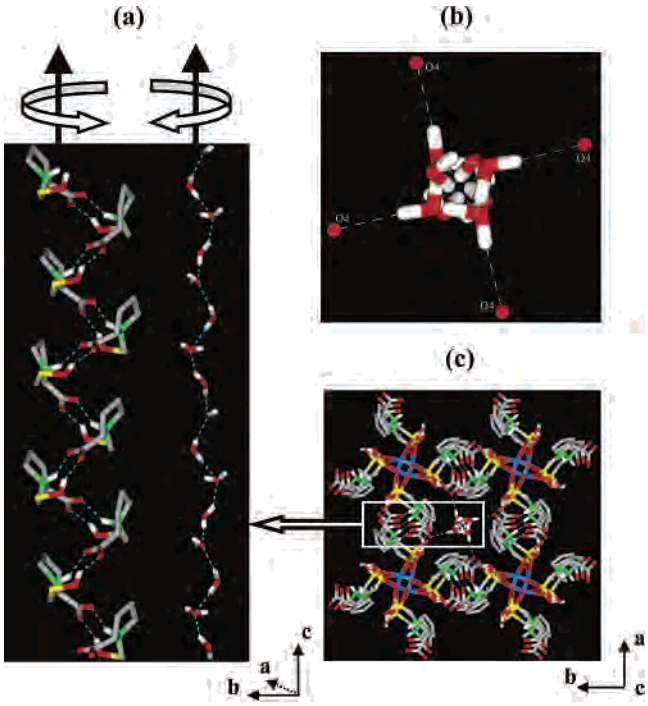

Figure 3. 1D hydrogen-bonded right-handed helical host chain (left) and the 1D left-handed helical water chain (right) running along the *c* axis (a), the anchoring of the water chain to the noncoordinating carboxylate oxygen atoms of the helical host chain through hydrogen bonds (b), and a view of the 1D helical water chain in the 1D channel formed from four adjacent triple-stranded helical chains (c). The arrows in panel a indicate the helicity of the host and the water chains; the hydrogen atoms attached to carbon atoms are omitted for clarity, and the hydrogen bonds are represented by the dotted lines: Tb, blue; P, yellow; C, gray; N, green; O, red; H, white.

and the slight difference in vibrational frequency is attributable to variation of the microenvironment for the water chain and for liquid water.

Although compounds **2**, **3**, and **4** are isostructural with **1**, differences do exist for these four compounds. As shown in Tables 2−5, the metal−oxygen bond distances and angles for compounds **2**, **3,** and **4** vary from compound to compound because the radii of the Ln(III) ions are different.

Thermal Properties. Thermogravimetric curves have been obtained in air for crystalline samples of the four compounds in the temperature range of 35−800 °C. The TG curve of **1** shows two main weight losses (Figure S2). The first weight loss of 2.24% from 35 to 315 °C corresponds to removal of one lattice water molecule in each formula unit (calcd 2.20%). It is presumable that the other water molecule in the formula unit is lost during the sample preparation for the TG analysis because the TG sample chamber is rather dry. The second weight loss occurs in the temperature range of 315−440 °C, attributable to the decomposition of the organic groups. The final residual of the thermal process is a mixture of $TbPO_4$ and Tb_2O_3 on the basis of powder X-ray diffraction. The observed total weight loss of 34.26% is less than the theoretical value (37.81%) because the thermal decomposition process is not complete at 800 °C, as shown by the slope of the curve. When the as-synthesized sample was subjected to heating at 250 °C for 2 h under vacuum in the electrogravimetric balance, the weight loss appeared to be 4.43%, suggesting that the guest water molecules are completely removed (ca. 4.37%). This phenomenon indicates that the guest water molecules can be easily removed from the host channels under vacuum. The powder XRD patterns demonstrate the retention of the framework structure of **1** after the removal of both lattice water molecules at 250 °C in a vacuum (Figure S3). The TG analysis results of **1**, **2**, **3**, and **4** are almost identical, indicating that the thermal behaviors of the four compounds are very similar because of isostructuralism.

Photoluminescent Properties. The photoluminescent spectra of the as-synthesized samples of **1** and **3** are measured at room temperature. As shown in Figure 4a, the free H_3L exhibits fluorescent emission bands at 371 and 425 nm (λ_{ex} = 235 nm), which are attributable to the $\pi^* \rightarrow \pi$ and $\pi^* \rightarrow$ n transitions, respectively. Upon bonding of the H_3L with the lanthanide ions, the luminescent spectra of the compounds formed display emission bands characteristic of the corresponding lanthanide ions, whereas the emissions arising from the free H_3L are not observable. The absence of the free H_3L emissions in compounds **1** and **3** suggests energy transfer from the phosphonate group to the central metal ions during photoluminescence. When **1** is excited at 249 nm, emissions appear in the range of 450−650 nm, and these emissions are attributed to the $^5D_4 \rightarrow {}^7F_J$ (J = 6, 5, 4, 3) transitions of Tb(III) ion (Figure 4b). The $^5D_4 \rightarrow {}^7F_6$, $^5D_4 \rightarrow {}^7F_5$, and $^5D_4 \rightarrow {}^7F_4$ emission bands each split into two peaks (481 and 488, 540 and 548, and 582 and 595 nm, respectively), corresponding to crystal field splitting. The $^5D_4 \rightarrow {}^7F_6$ and $^5D_4 \rightarrow {}^7F_5$ emissions result from an electric dipole transition and a magnetic dipole transition, respectively. The spectrum is dominated by the $^5D_4 \rightarrow {}^7F_5$ transition which is more intense than the others, resulting in a strong green luminescence output for the solid sample. When the Eu(III) compound (**3**) is excited at 248 nm, characteristic luminescent bands appear at 588, 596, 611, 652, and 700 nm via the ligand-to-metal energy transfer mechanism, which correspond to the transitions from the $^5D_0$ state to the ^7F_J (J = 0−4) levels, respectively (Figure 4c). Among these transitions, the $^5D_0 \rightarrow {}^7F_2$ transition, which is an electric dipole transition and is extremely sensitive to chemical bonds in the vicinity of Eu(III) ion, is the strongest one, leading to bright red luminescence. It is known that the intensity of the $^5D_0 \rightarrow {}^7F_2$ transition increases as the site symmetry of Eu(III) decreases, whereas the $^5D_0 \rightarrow {}^7F_0$ transition is strictly forbidden in a field of symmetry. Only one sharp, the second most intense, band (588 nm) is observed for the $^5D_0 \rightarrow {}^7F_0$ zero-phonon line in **3**. The photoluminescence results reveal not only the noncentrosymmetry of Eu(III) but also the presence of only one type of Eu(III) site in the unit cell of **3**. This is consistent with the result of the single-crystal X-ray analysis. The $^5D_0 \rightarrow {}^7F_1$ transition is a magnetic dipole transition; its intensity varies with the crystal field strength around the Eu(III) ion, and the intensity of this transition in **3** is weak. The intensity ratio of the $^5D_0 \rightarrow {}^7F_2$ transition to the $^5D_0 \rightarrow {}^7F_1$ one is widely used as a measure of the

(43) Neogi, S.; Bharadwaj, P. K. *Inorg. Chem.* **2005**, *44*, 816.

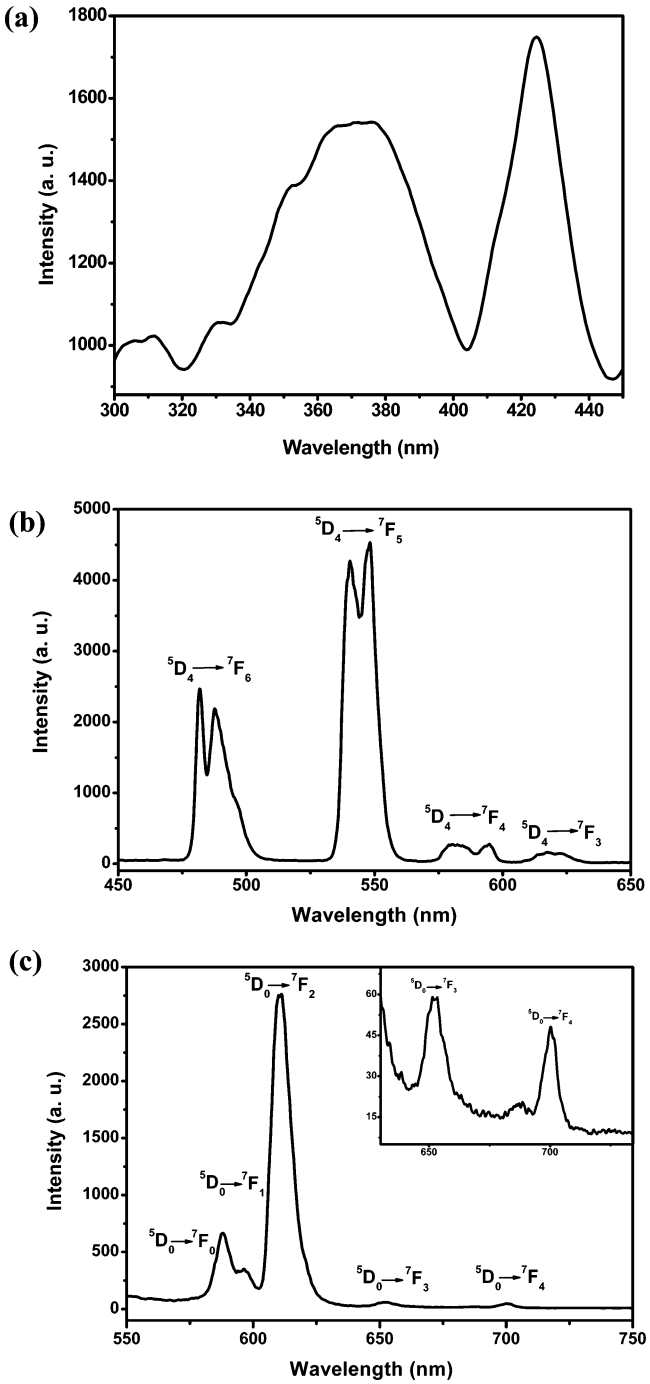

Figure 4. Emission spectrum of free H_3L in the solid state at room temperature, $\lambda_{exc} = 235$ nm (a), the emission spectrum of **1** corresponding to the $^5D_4 \rightarrow {}^7F_J$ ($J = 6, 5, 4, 3$) transitions in solid state at room temperature, $\lambda_{exc} = 249$ nm (b), and the emission spectrum of **3** corresponding to the $^5D_0 \rightarrow {}^7F_J$ ($J = 0, 1, 2, 3, 4$) transitions in solid state at room temperature, $\lambda_{exc} = 248$ nm (c).

coordination state and the site symmetry of the rare earth.[44] For **3**, the intensity ratio $I(^5D_0 \rightarrow {}^7F_2)/I(^5D_0 \rightarrow {}^7F_1)$ is about 4.6, also indicating that the Eu(III) ions are not in an inversion center in **3**.

Adsorption Properties. To determine if these structures have architectural rigidity and permanent porosity, we have measured the N_2, as well as H_2O, CH_3OH, and CH_3CH_2OH,

(44) Xu, Q. H.; Li, L. S.; Liu, X. S.; Xu, R. R. *Chem. Mater.* **2002**, *14*, 549.

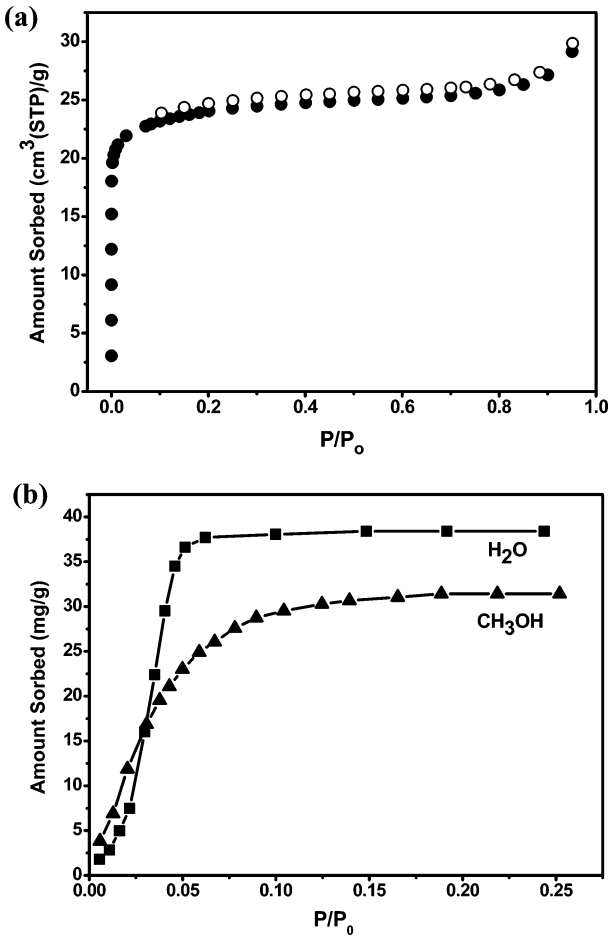

Figure 5. N_2 adsorption isotherm for **2** at 77 K (a) (branches are represented by the filled and open circles, respectively) and the H_2O and CH_3OH sorption isotherms for **1** at 298 K (b).

adsorption isotherms. Here, only the adsorption properties of **2** are described in detail because compounds **1**−**4** are isostructural to one another and their adsorption behaviors are similar. As shown in Figure 5, the N_2 sorption of **2** at 77 K shows a reversible type-I isotherm, characteristic of a microporous material and indicative of the permanent microporousity and architectural stability of the evacuated framework. The N_2 uptake of 29.14 cm^3 (STP)/g (36.63 mg/g) corresponds to 1.1 N_2 molecules per formula unit of the compound. With the BET model, the apparent surface area of **2** is calculated to be 80.93 m^2/g. By extrapolation of the Dubinin−Radushkevich (DR) equation, the pore volume is estimated to be 0.029 cm^3/g. This smaller pore volume is reasonable because the 3D supramolecular framework of **2** has only one-dimensional channels along the *c* axis. Compound **2** also shows type-I isotherms upon exposure to H_2O and CH_3OH vapors at 298 K (Figure 5). The H_2O uptake of 38.41 mg/g amounts to 1.76 H_2O molecules per formula unit, which is in agreement with the theoretical value. The CH_3OH uptake of 31.43 mg/g is equivalent to 0.8 CH_3OH molecules per formula unit. These results reveal that N_2, H_2O, and CH_3OH molecules can diffuse inside the micropores of **2**. The powder XRD patterns indicate that **2** maintains its structural integrity after dehydration−rehydration cycles. Despite the stable framework structure, no CH_3CH_2OH

sorption capacity for **2** was observed at 298 K. The selective sorption of N_2, H_2O, and CH_3OH may be attributed to the small aperture of the channels in **2**, which discriminates these molecules with small kinetic diameters. To the best our knowledge, compounds **1**−**4** are the first homochiral porous lanthanide phosphonates exhibiting permanent porosity for selective sorption of molecules.

Conclusions

Four isostructural homochiral porous lanthanide phosphonates with one-dimensional triple-strand helical chains have been crystallized from a hydrothermal reaction system using enantiomerical *N*-(phosphonomethyl)proline as the building unit. These compounds show an interesting 3D supramolecular framework structure with channels formed by helical chains, and they exhibit selective adsorption capacities after removal of the guest water molecules in the channels. The successful preparation of the four solid compounds, **1**−**4**, provides valuable information for further construction of other homochiral porous lanthanide phosphonate frameworks. Such chiral porous materials hold promise in applications such as enantioselective separation and heterogeneous asymmetric catalysis.

Acknowledgment. This work was supported by the National Natural Science Foundation of China and the Education Ministry of China.

Supporting Information Available: Four crystallographic tables and X-ray crystallographic files (CIF), FTIR spectra and TG-DTA curves for compounds **1**, **2**, **3**, and **4**, the powder XRD patterns of the samples after removal of lattice water molecules at 250 °C in a vacuum for **1,** and the interatomic distances and angles for the hydrogen bonding interactions for compounds **2**, **3**, and **4**. This material is available free of charge via the Internet at http://pubs.acs.org.

IC060162H